

# A Transfer Learning-Based Method for Water Body Segmentation in Remote Sensing Imagery: A Case Study of the Zhada Tulin Area

Haonan Chen <sup>1</sup> and Xin Tong <sup>2\*</sup>

<sup>1</sup>Engineering College, Tibet University, Lhasa, 850000, China.

<sup>2\*</sup>School of Physical Science and Technology, Northwestern Polytechnical University, Xi'an, 710072, China.

\*Corresponding author(s). E-mail(s): [tongxin@mail.nwpu.edu.cn](mailto:tongxin@mail.nwpu.edu.cn);  
Contributing authors: [19904389365@163.com](mailto:19904389365@163.com);

## Abstract

To address the prevalent challenges of domain shift and small sample sizes in remote sensing image water body segmentation, this study proposes and validates a two-stage transfer learning strategy based on the SegFormer model. The approach begins by training a foundational segmentation model on a diverse source domain, where it achieves an Intersection over Union (IoU) of 68.80% on its validation set, followed by fine-tuning on data from the distinct target domain. Focusing on the Zhada Tulin area in Tibet—a region characterized by highly complex topography and spectral features—the experimental results demonstrate that this strategy significantly boosts the IoU for the water body segmentation task from 25.50% (for direct transfer) to 64.84%. This not only effectively resolves the model performance degradation caused by domain discrepancy but also provides an effective technical paradigm for high-precision thematic information extraction in data-scarce and environmentally unique remote sensing scenarios.

**Keywords:** Remote sensing imagery, Water body segmentation, Transfer learning, SegFormer, Domain shift, Zhada Tulin

# 1 Introduction

The accurate acquisition of spatial information on water bodies, as one of the most crucial natural elements on the Earth’s surface, is of great significance for water resource management, ecological environment protection, and disaster risk assessment. In recent years, with the continuous development of remote sensing technology, high-resolution satellite imagery has provided powerful support for large-scale water body monitoring. However, traditional water extraction methods, such as the Normalized Difference Water Index (NDWI) (McFeeters, 1996; Xu, 2006), the Automated Water Extraction Index (AWEI) (Feyisa et al., 2014), threshold segmentation (Otsu et al., 1975), and active contour models (Kass et al., 1988), often struggle to achieve satisfactory results in complex surface environments, especially in areas where the spectral characteristics of water bodies are similar to the background and the terrain is complex. These traditional methods often require assistance from other indices, such as the Normalized Difference Vegetation Index (NDVI) (Rouse Jr et al., 1973) and the Soil-Adjusted Vegetation Index (SAVI) (Huete, 1988), to differentiate water from other features.

The rise of deep learning technology has brought new opportunities for water body extraction from remote sensing imagery (Goodfellow et al., 2016; Zhu et al., 2017; Ma et al., 2019; Zhang et al., 2016). Convolutional Neural Networks (CNNs) (LeCun et al., 2002), with their powerful feature learning capabilities, have shown excellent performance in various remote sensing applications. Early Fully Convolutional Networks (FCNs) (Long et al., 2015) laid the foundation for pixel-level semantic segmentation. Subsequently, foundational architectures like U-Net (Ronneberger et al., 2015), SegNet (Badrinarayanan et al., 2017), and the DeepLab series (Chen et al., 2017, 2018) significantly improved segmentation accuracy by integrating techniques like atrous (dilated) convolutions (Yu and Koltun, 2015) and powerful backbones like ResNet (He et al., 2016). More recently, Transformer-based models like SegFormer (Xie et al., 2021), leveraging the global modeling capabilities of the attention mechanism (Vaswani et al., 2017) and advantages in multi-scale feature fusion, have shown particularly outstanding performance in semantic segmentation tasks. Hierarchical vision transformers like the Swin Transformer (Liu et al., 2021) have further advanced the field. These methods can automatically learn complex spatio-spectral features, significantly enhancing the accuracy and robustness of water body identification.

However, the success of deep learning models heavily relies on a large amount of high-quality annotated data. In the remote sensing domain, this requirement faces practical challenges: the acquisition of high-quality imagery is constrained by various factors, and precise pixel-level annotation is not only time-consuming but also requires extensive expertise. More critically, imaging conditions and feature characteristics vary significantly across different geographical regions, causing models trained in one area to experience a sharp performance decline when directly applied to another—a phenomenon widely known as "domain shift" in computer vision.

To mitigate these issues, transfer learning offers an effective pathway (Pan, 2010; Yosinski et al., 2014). By transferring knowledge learned from a data-rich source domain to a data-scarce target domain, it is possible to achieve better model performance with limited annotated samples. In the field of natural image processing,

the "pre-train and fine-tune" paradigm based on ImageNet pre-training has become a standard practice (Krizhevsky et al., 2017). However, remote sensing images possess unique spectral properties, spatial resolutions, and feature distribution patterns, making the simple application of transfer learning strategies from natural images often yield limited results (Tuia et al., 2016). How to design effective transfer learning methods tailored to the characteristics of remote sensing applications remains a question worthy of in-depth exploration. In recent years, researchers have explored various deep learning methods for remote sensing image analysis, including multi-attention networks (Li et al., 2021), building extraction with sparse tokens (Chen et al., 2021), Local Attention Embedding Network (LANet) (Zhang et al., 2021), and hybrid Transformer-CNN networks (Zhang et al., 2022), all of which have achieved good results in different applications. Meanwhile, methods like non-local neural networks (Wang et al., 2018) and scene classification frameworks (Thapa et al., 2023) have also provided new insights for remote sensing image understanding.

The Zhada Tulin in the Ali Prefecture of Tibet is a unique geomorphological landscape on the Qinghai-Tibet Plateau, and its associated gully water systems exhibit typical characteristics of a high-altitude arid region. Due to special geological structures and climatic conditions, water bodies in this area are characterized by small scales, irregular shapes, and significant seasonality. Furthermore, their spectral features are heavily influenced by sediment content, making them easily confused with the surrounding earth forest landscape. These factors pose a great challenge for water body extraction in the Zhada area, making it an ideal testbed for evaluating the performance of water segmentation algorithms. At the same time, remote sensing data for this region is relatively scarce, and labeled samples are limited, which aligns with the "small-sample" scenario often encountered in practical applications.

Against this background, this study designs a two-stage transfer learning strategy for remote sensing water body segmentation. We first construct a large-scale source domain dataset containing diverse geographical environments to train a base model with good generalization capabilities. Then, we use a small amount of labeled data from the Zhada Tulin area to fine-tune the model, enabling it to adapt to the specific water body characteristics of the target region. Through this "general-to-specific" learning strategy, we expect to achieve high-precision water body segmentation under small-sample conditions. This research not only provides technical support for water information extraction in the Zhada region but also offers a valuable exploration for the application of transfer learning in remote sensing thematic information extraction.

## 2 Study Area and Methods

To systematically evaluate the effectiveness of a two-stage transfer learning strategy for remote sensing water body segmentation, this study established a data scheme involving a diverse source domain and a unique target domain, along with corresponding procedures for model training, implementation, and evaluation.

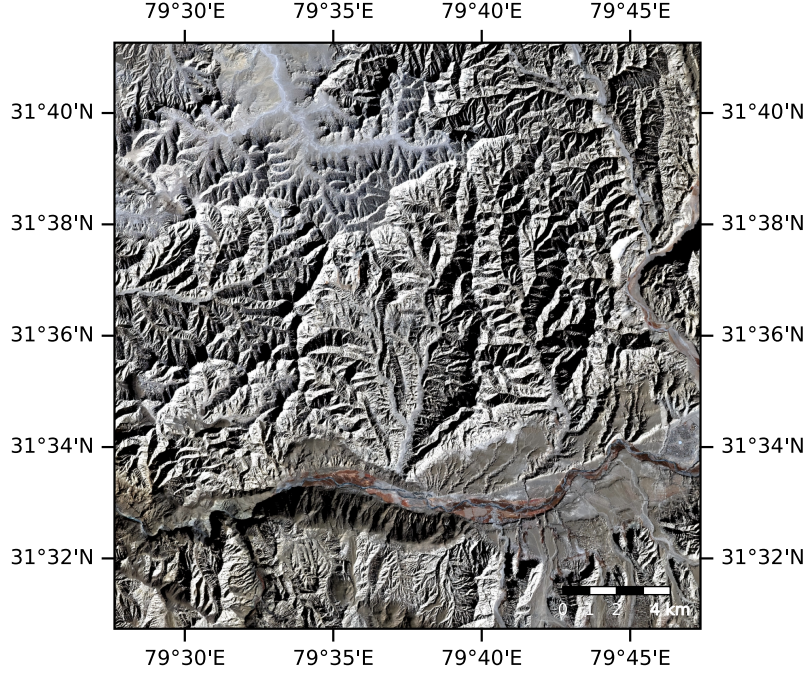


**Fig. 1** Geographic location map of the study areas, highlighting the target domain in the Zhada Tulin area.

## 2.1 Study Area and Datasets

The datasets for this study consist of a diverse source domain (Dataset A) and a highly challenging target domain (Dataset B).

The source domain (Dataset A) was constructed to provide rich and generalizable learning samples for pre-training the foundational model. The imagery for this dataset is primarily sourced from China’s Gaofen-7 (GF-7) satellite, whose sub-meter high resolution (0.8-meter panchromatic and 3.2-meter multispectral) provides an excellent data foundation for fine-grained feature recognition. The spatial coverage of the source domain is extensive, focusing on diverse plateau and mountainous environments. It not only includes several typical regions in western China (such as arid lakes in Xinjiang, salt lakes in Qinghai, and plateau lakes in Tibet) but also encompasses mountain lakes and glacial meltwater rivers in the Rocky Mountains of the United States. The variety of water body types is extremely rich, including large plateau lakes, inland rivers, glacial meltwaters, and mountain valleys. This high degree of diversity in space and water body types ensures that a model trained on this dataset can learn universal features of water bodies and possess good generalization potential.

The target domain (Dataset B) focuses on a highly challenging geographical unit—the Zhada Tulin (Zhada Earth Forest) in the Ali Prefecture of Tibet, China (Fig. 1). The imagery for this region is sourced from the Gaofen-2 (GF-2) satellite. Its resolution is consistent with that of GF-7, ensuring scale consistency for cross-dataset comparison. Located in the upper reaches of the Yarlung Zangbo River, the Zhada



Tulin is a typical high-altitude arid region, and its hydrological environment differs significantly from the source domain: (1) **Unique Morphology:** The water systems flow through narrow gullies within the unique "earth forest" landscape, exhibiting irregular shapes and significant seasonal variations. (2) **High Turbidity:** The rivers carry large amounts of sediment, causing their spectral characteristics to differ vastly from the clear water bodies in the source domain. (3) **Complex Background:** The water bodies are highly coupled with the surrounding exposed sediments, both geomorphologically and spectrally, which can easily confuse segmentation algorithms. The unique geographical environment, hydrological features, and different sensor origins of the target domain collectively constitute a significant domain shift, making it an ideal testbed for validating the effectiveness of the proposed transfer learning strategy.

## 2.2 Two-Stage Transfer Learning Framework

To address the domain shift problem and leverage prior knowledge to enhance segmentation accuracy in the small-sample region, this study designed a two-stage transfer learning framework, as illustrated in Fig. 2. The core idea of this framework is to first train a robust foundational model (Model A1) on a feature-rich source domain dataset, and then use it as a pre-trained model for fine-tuning on the small-sample target domain dataset to obtain a final, high-precision model (Model A2) adapted to the target region. The main steps are as follows:

1. **Stage 1: Source-Domain Pre-training.** The SegFormer model is thoroughly trained using the source domain dataset (Dataset A). The objective of this stage is to enable the model to learn universal spatial and textural features of water bodies, resulting in a foundational model (Model A1) with strong generalization capabilities. To accelerate convergence, the encoder component is initialized with ImageNet pre-trained weights.
2. **Stage 2: Target-Domain Fine-tuning.** All weights of the foundational model A1 are used as initialization parameters for a new model. This model is then secondarily trained (fine-tuned) on the limited-sample target domain dataset (Dataset B). This stage aims to adapt the model to the specific visual characteristics and complex background of the target domain, ultimately producing an optimized segmentation model (Model A2) for the Zhada Tulin area.
3. **Model Performance Evaluation.** To validate the effectiveness of the proposed strategy, a comprehensive quantitative and qualitative evaluation is conducted on the validation set of the target domain. The performance of the directly transferred model (A1), a baseline model trained from scratch, and the fine-tuned final model (A2) are rigorously compared.

To implement this framework, all original remote sensing images must undergo a standardized sample construction process (Fig. 3). This process involves two main steps: sliding window cropping and data augmentation, designed to convert the raw data into patches suitable for model training.

To ensure data quality and simulate real-world challenges, we retained the inherent radiometric differences between the GF-7 and GF-2 raw data products without additional calibration. This approach preserves the natural spectral variations across

sensors, enhancing the model’s robustness in practical multi-source remote sensing applications where data fusion from different satellites is common.

**Sliding Window Cropping.** To standardize the input size and effectively augment the number of samples, this study employs an overlapping sliding window method to synchronously crop the original images and their corresponding vector label maps. Specifically, a  $512 \times 512$  pixel window (Fig. 3b) is moved across the image with a stride of 128 pixels (i.e., a 25% overlap). The overlap ensures the integrity of features across different samples and avoids the loss of boundary information caused by hard cutting. After cropping, only image patches containing water pixels and their corresponding labels are retained to build an effective training set.

**Data Augmentation.** To enhance the model’s generalization ability and effectively mitigate overfitting, a series of data augmentation techniques (Fig. 3c-f) are applied exclusively during the training phase. The employed strategies include:

- *Geometric transformations:* Random horizontal flipping, and random scaling (with a factor in the range  $[0.5, 2.0]$ ) followed by a random crop back to  $512 \times 512$  pixels.
- *Photometric distortions:* Random adjustments to the brightness, contrast, and saturation of the image to simulate different lighting and atmospheric conditions.

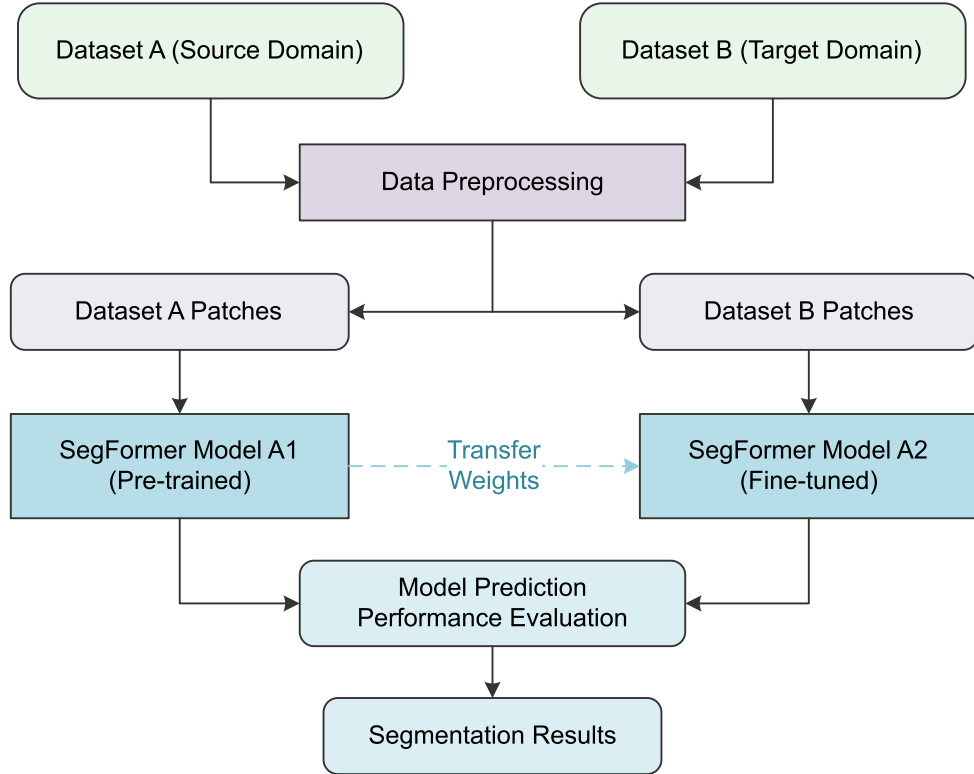


**Fig. 2** The overall technical framework of the two-stage transfer learning strategy.

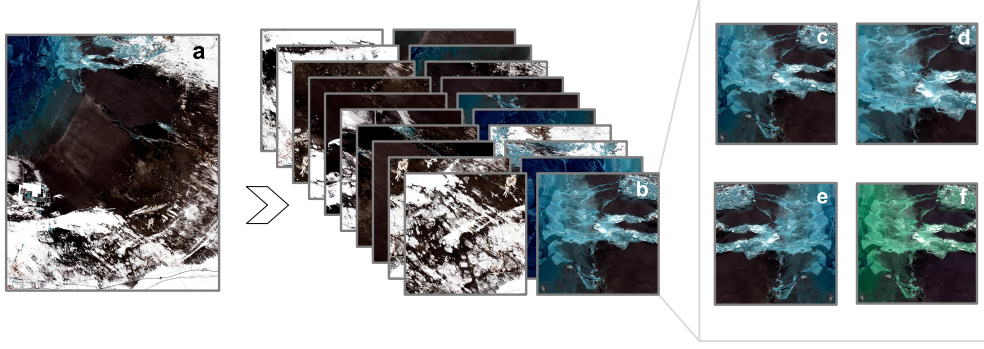


**Fig. 3** Diagram of the data preprocessing pipeline: (a) Original remote sensing image; (b) Sliding window cropping into  $512 \times 512$  patches; (c)-(f) Data augmentation on training samples.

These operations enable the model to learn more robust, deep features of water bodies that are invariant to changes in scale, angle, and illumination.

Through this sample construction pipeline, the final training and validation sets for the source and target domains were obtained. Specifically, 3,875 valid  $512 \times 512$  pixel patches were cropped from 207 original GF-7 images for the source domain (Dataset A), while 180 patches were obtained from 20 original GF-2 images for the target domain (Dataset B). Subsequently, to ensure an objective and consistent evaluation, both datasets were randomly split into training and validation sets at a 9:1 ratio. It is noteworthy that the training set for the target domain B contains only 162 samples ( $180 \times 0.9$ ), which further highlights the "small-sample" challenge in this specific region and underscores the necessity of the proposed transfer learning strategy.

### 2.3 Semantic Segmentation Model

This study selected SegFormer (Xie et al., 2021) as the core semantic segmentation network for the precise extraction of water bodies from remote sensing imagery. SegFormer is a highly efficient model based on a pure Transformer architecture, striking an excellent balance between accuracy and efficiency, making it particularly suitable for processing high-resolution remote sensing images. The model primarily consists of a hierarchical Transformer encoder and a lightweight all-MLP (Multilayer Perceptron) decoder head, as shown in Fig. 4.

The encoder of SegFormer employs the Mix Transformer (MiT) (Cui et al., 2022) series as its backbone; this study specifically uses the MiT-B5 version. Unlike the traditional Vision Transformer (ViT) (Dosovitskiy et al., 2020), MiT achieves efficient multi-scale feature extraction. It can effectively extract feature representations at different scales from the input image, which is crucial for identifying water bodies of various sizes and shapes. Through an improved self-attention mechanism and a position-encoding-free design, MiT significantly enhances computational efficiency and adaptability to different input sizes. This design paradigm, which has seen successful application in remote sensing image processing (Wang et al., 2022), is well-suited for handling the complex spatial relationships within remote sensing images.

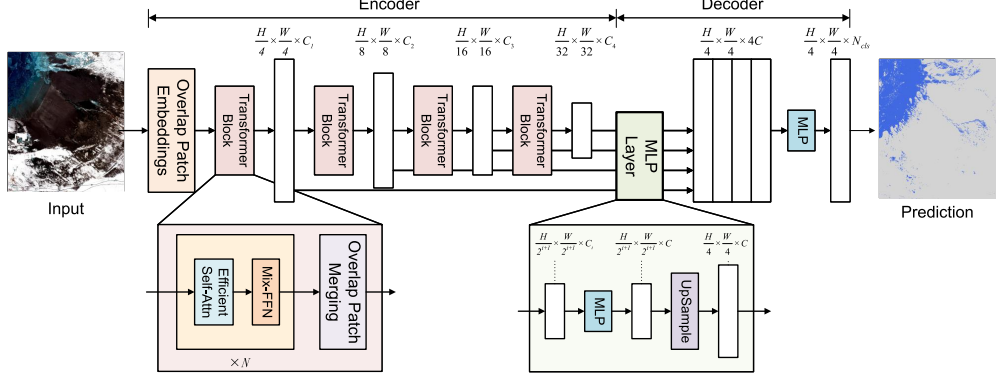


**Fig. 4** Architecture of SegFormer, including a hierarchical Transformer encoder and an all-MLP decoder (Xie et al., 2021).

For the decoder, SegFormer innovatively uses a very simple all-MLP head. This decoder head can efficiently aggregate the multi-level features output by the encoder and generate the final pixel-level segmentation map with low computational cost.

By virtue of its powerful multi-scale feature capturing capabilities, excellent computational efficiency, and robust support for high-resolution inputs, SegFormer was chosen as the foundational model for the water body segmentation and subsequent transfer learning exploration in this study.

## 2.4 Model Training and Implementation

The implementation and training of all models in this study were conducted based on the PyTorch (Paszke, 2019) deep learning framework within a unified hardware environment to ensure the comparability of the results.

To effectively guide the training process of the SegFormer model and address issues such as class imbalance (e.g., significantly more background pixels than water pixels) and ambiguous object boundaries in the water body segmentation task, this study employs a compound loss function. This loss is a linear combination of a weighted Cross-Entropy Loss and a Dice Loss (Milletari et al., 2016).

The Dice Loss originates from the Dice Similarity Coefficient (DSC) and directly measures the overlap between the model’s prediction and the ground truth. It is inherently robust to class imbalance and performs well in optimizing segmentation boundaries. The inclusion of Dice Loss encourages the model to generate results with better spatial continuity and clearer boundaries. Its formula is as follows:

$$\mathcal{L}_{\text{Dice}} = 1 - \frac{2 \sum_{i=1}^N p_i y_i + \varepsilon}{\sum_{i=1}^N p_i + \sum_{i=1}^N y_i + \varepsilon} \quad (1)$$

where  $\mathcal{L}_{\text{Dice}}$  is the continuous form of the Dice loss;  $p_i \in [0, 1]$  is the probability predicted by the model for the positive class at pixel  $i$ ;  $y_i \in \{0, 1\}$  is the ground truth

label for pixel  $i$ ;  $N$  is the total number of pixels; and  $\varepsilon$  is a smoothing term to prevent division by zero.

The Cross-Entropy Loss (Zhang and Sabuncu, 2018), a standard pixel-level classification loss for image segmentation, aims to minimize the difference between the predicted pixel class probability distribution and the ground truth. To further mitigate the imbalance between foreground (water) and background pixels, different weights were assigned to each class. Specifically, the weight for the background class was 0.2289, and for the water class, it was 0.7711. By assigning a higher loss weight to the less frequent water class, the model is guided to pay more attention to its correct identification. For our binary semantic segmentation task, the formula is:

$$\mathcal{L}_{\text{BCE}} = -\frac{1}{N} \sum_{i=1}^N [y_i \log(p_i) + (1 - y_i) \log(1 - p_i)] \quad (2)$$

where  $\mathcal{L}_{\text{BCE}}$  is the binary cross-entropy for our task. This study aims to leverage the advantages of both cross-entropy loss in pixel-wise classification and Dice loss in handling class imbalance and optimizing regional overlap, thereby enhancing the overall segmentation performance.

The core training parameters are configured as follows:

1. **Optimizer:** The AdamW optimizer (Loshchilov and Hutter, 2017) was used with an initial learning rate set to  $6 \times 10^{-6}$  and a weight decay of 0.01.
2. **Learning Rate Schedule:** The training was conducted for a total of 20,000 iterations. A learning rate schedule with a linear warm-up was employed (the learning rate linearly increased from a factor of  $1 \times 10^{-6}$  of the initial learning rate to the initial learning rate over the first 1,500 iterations), followed by a polynomial decay until the end of training (with a minimum learning rate of  $1 \times 10^{-5}$ ).
3. **Batch Size:** Set to 6.

## 2.5 Performance Evaluation Metrics

To comprehensively and objectively evaluate the performance of the different models in segmenting water bodies from remote sensing imagery, a series of standard metrics widely used in the field of semantic segmentation were selected. These metrics measure the consistency between the model’s predictions and the ground truth from various dimensions. They are typically calculated based on four fundamental quantities for a binary classification problem (water and background):

- **True Positives (TP):** The number of water pixels correctly predicted as water.
- **False Positives (FP):** The number of background pixels incorrectly predicted as water (misdetections).
- **True Negatives (TN):** The number of background pixels correctly predicted as background.
- **False Negatives (FN):** The number of water pixels incorrectly predicted as background (missed detections).

The specific evaluation metrics are defined as follows:

1. **Intersection over Union (IoU):** Measures the overlap between the predicted segmentation area and the ground truth area. It is one of the most commonly used core metrics in semantic segmentation.

$$\text{IoU} = \frac{\text{TP}}{\text{TP} + \text{FP} + \text{FN}} \quad (3)$$

2. **Precision (P):** Represents the proportion of pixels correctly identified as water among all pixels predicted as water (also known as correctness).

$$\text{Precision} = \frac{\text{TP}}{\text{TP} + \text{FP}} \quad (4)$$

3. **Recall (R):** Represents the proportion of actual water pixels that were correctly identified by the model (also known as completeness).

$$\text{Recall} = \frac{\text{TP}}{\text{TP} + \text{FN}} \quad (5)$$

4. **F1-score:** The harmonic mean of Precision and Recall, used to measure the overlap between the prediction and the ground truth.

$$\text{F1-score} = 2 \times \frac{\text{Precision} \cdot \text{Recall}}{\text{Precision} + \text{Recall}} \quad (6)$$

## 3 Results

### 3.1 Source Domain Model Performance

To ensure the effectiveness of the subsequent transfer learning, the performance of the foundational model A1, trained on the source domain dataset A, was first evaluated. The segmentation performance of Model A1 on the validation set of the source domain is shown in Table 1.

**Table 1** Performance of the source domain model A1 on its validation set.

Class	IoU (%)	F1-score (%)	Precision (%)	Recall (%)
Background	88.63	93.97	94.26	93.69
Water	68.80	81.52	80.77	82.28

As can be seen from Table 1, the foundational model A1 achieved good segmentation results on its validation set. For the critical "Water" class, the Intersection over Union (IoU) reached 68.80%, and the F1-score reached 81.52% (note: in binary semantic segmentation, the F1-score is equivalent to the Dice coefficient). The precision and recall were 80.77% and 82.28%, respectively. These metrics indicate that



Model A1 has developed strong generalization capabilities, laying a solid foundation for the subsequent knowledge transfer to the target domain.

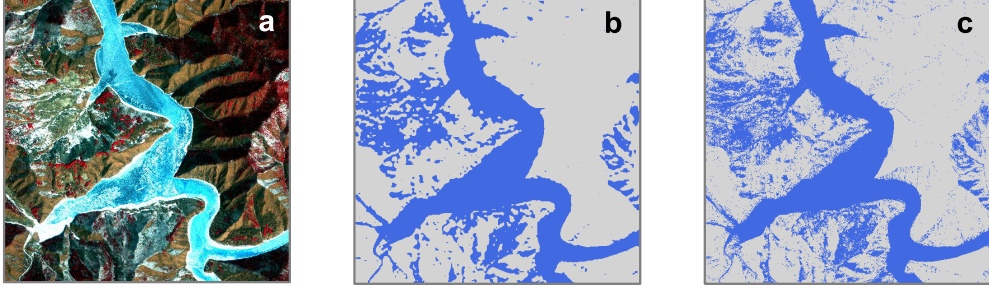


**Fig. 5** Segmentation results of the foundational model A1 on a typical scene from the source dataset A: (a) Original Image, (b) Ground Truth, (c) Prediction of Model A1.

Figure 5 displays the segmentation results of the foundational model A1 in a typical scene from the source domain, aiming to visually assess its performance as a starting point for transfer. In this scene’s remote sensing image (Fig. 5a), the water-land boundary is clear, providing a good basis for model learning. By comparing the prediction (Fig. 5c) with the ground truth (Fig. 5b), it is evident that the predicted contours highly coincide with the actual water boundaries, demonstrating excellent pixel-level segmentation accuracy. It is noteworthy that the model not only accurately delineated the meandering form of the main river channel but also successfully captured the small tributary flowing into it, indicating a good understanding of the spatial connectivity and structural hierarchy of the water system.

### 3.2 Comparative Analysis of Transfer Learning

To comprehensively evaluate the effectiveness of the proposed transfer learning strategy, a rigorous quantitative and qualitative comparison of models trained under different strategies was conducted on the validation set of the target domain (Dataset B). The strategies include: 1) **Direct Transfer**, where the foundational model A1 (SegFormer) trained on the source domain was directly applied to the target domain; 2) **Train from Scratch with SegFormer** (B-scratch (Seg)), using ImageNet pre-trained weights as initialization but trained solely on the target domain; 3) **Train from Scratch with U-Net** (B-scratch (U-Net)), a simpler baseline model trained from random initialization on the target domain; and 4) **Transfer Learning** (A2), the proposed strategy of fine-tuning Model A1 on the target domain.

The updated results, as shown in Table 2, reveal performance differences across strategies. The direct transfer model (A1) performed the poorest, with a water IoU of 25.50% and a recall of 28.76%. This drop (compared to its 68.80% IoU in the source domain) highlights the domain shift issue.

**Table 2** Performance comparison of the models on the validation set of target dataset B.

Model	Class	IoU (%)	F1-score (%)	Precision (%)	Recall (%)
A1 (Direct Transfer)	Background	72.06	83.76	75.25	94.43
	Water	25.50	40.64	69.24	28.76
B-scratch (SegFormer)	Background	69.58	82.06	77.38	87.35
	Water	37.47	54.51	64.40	47.26
B-scratch (U-Net)	Background	72.00	84.34	83.11	84.34
	Water	48.82	65.61	66.65	64.61
<b>A2 (Fine-tuned)</b>	Background	<b>77.59</b>	<b>87.38</b>	<b>89.80</b>	<b>85.09</b>
	Water	<b>64.84</b>	<b>78.67</b>	<b>75.25</b>	<b>82.42</b>

The SegFormer model trained from scratch (B-scratch (Seg)) achieved a water IoU of 37.47%. In comparison, the U-Net model trained from scratch (B-scratch (U-Net)) reached a water IoU of 48.82%.

The fine-tuned model (A2) achieved the highest performance, with a water IoU of 64.84%, representing a relative gain of approximately 154% over direct transfer, 73% over SegFormer scratch, and 33% over U-Net scratch.

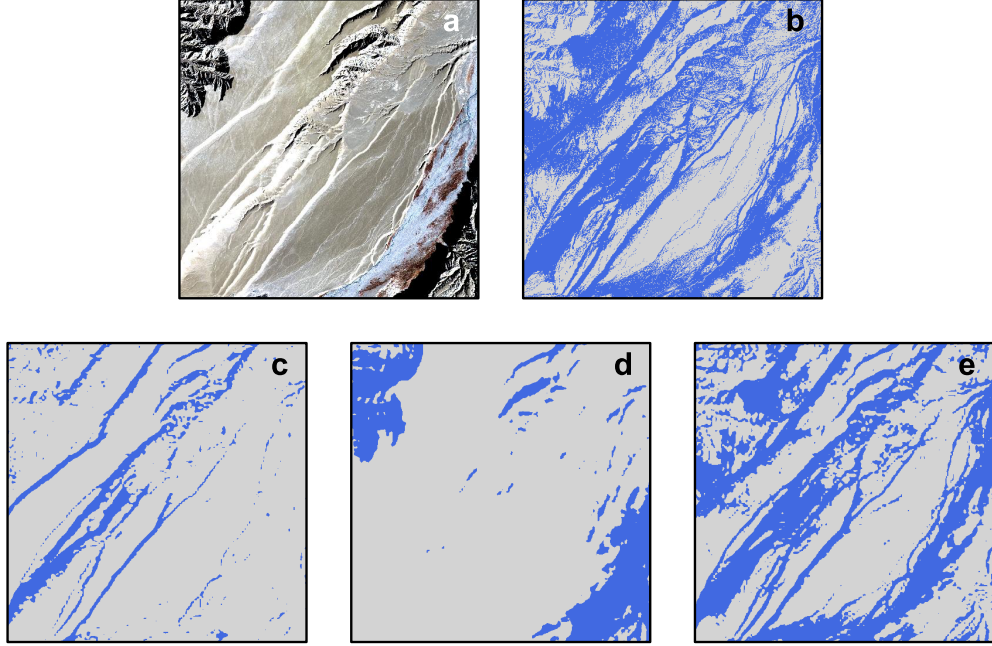
**Fig. 6** Segmentation comparison of different models on a typical scene from the target dataset B: (a) Original Image, (b) Ground Truth, (c) Prediction of Model A1 (Direct Transfer), (d) Prediction of Model B-scratch (SegFormer), (e) Prediction of Model A2 (Fine-tuned). The figure focuses on SegFormer-based strategies, with U-Net results provided quantitatively in the table.

Figure 6 provides a visual comparison in a challenging Zhada Tulin scene, where water and background spectra are highly similar. The direct transfer (c) shows fragmented errors, SegFormer scratch (d) misses some connectivity, and the fine-tuned A2 (e) restores the river morphology most accurately.

## 4 Discussion

Figure 6 compares the performance of three strategies in a typical Zhada Tulin scene, where the spectral features between water bodies and the background (Fig. 6a) are highly similar.

The result from directly applying the source domain model A1 (Fig. 6c) confirms the domain shift issue. The prediction consists of fragmented and disordered patches, losing the river’s overall morphology. This indicates that features learned by Model A1 in the source domain do not generalize well to the new scene.

The result from the SegFormer model trained from scratch (B-scratch (Seg)) (Fig. 6d) highlights the challenges of small-sample learning. With only 162 training samples, the model fails to learn robust features for distinguishing water from background, often misclassifying local non-essential elements (e.g., mountain shadows or sediment textures) as water. This leads to incomplete convergence and poor performance on both training and validation sets. For comparison, the U-Net model trained from scratch (B-scratch (U-Net)) (Ronneberger et al., 2015) achieved a water IoU of 48.82%, outperforming the SegFormer scratch result of 37.47%.

In contrast, the proposed transfer learning strategy (Model A2) produces better results (Fig. 6e). The predictions align closely with the ground truth (Fig. 6b), preserving the river’s structure, connectivity, and minimizing background misclassifications.

The experiments reveal a notable pattern: training the SegFormer model with ImageNet pre-trained weights on the target domain (B-scratch (Seg)) yields an IoU of 37.47%, lower than the 48.82% from the simpler U-Net trained from random initialization. This can be attributed to the small sample size in the Zhada dataset, where the complex Transformer architecture of SegFormer struggles with limited data, resulting in suboptimal fitting. The U-Net, with its simpler CNN structure, shows greater robustness under such constraints.

However, both baselines underperform compared to the proposed transfer learning model A2 (IoU=64.84%). This underscores that model architecture alone—whether SegFormer or U-Net—cannot address the core issues. The key lies in the two-stage paradigm, which transfers domain-specific knowledge from dataset A to enhance the SegFormer model, overcoming small-sample and domain shift limitations. This approach offers a straightforward alternative to more intricate domain adaptation techniques, requiring fewer unlabeled samples.

The study’s outcomes stem from the transfer learning strategy’s role in knowledge reconstruction (Pan, 2010; Yosinski et al., 2014). Stage 1 pre-training equips Model A1 with general low-level features (e.g., color, texture, edges) from diverse source data. Direct application to Zhada Tulin, however, falls short due to unique local characteristics. Stage 2 fine-tuning adapts high-level semantics using targeted target-domain samples, enabling the model to handle specific distributions like sediment-influenced

spectra and complex backgrounds. Radiation differences between GF-7 and GF-2 data were retained to mimic real sensor variations, improving method robustness.

It is important to note that the source domain imagery was not pristine; many images contained significant masked-out regions, typically corresponding to cloud cover, cloud shadows, or sensor artifacts. These areas, visually distinct and containing no valid data values, increase the complexity of the training environment. The model must not only learn to identify water bodies but also to effectively ignore these large, irregular "no-data" zones, which adds to the challenge of learning robust and generalizable features and makes the pre-trained model more resilient to real-world data imperfections.

**Practical Implications and Limitations.** Beyond its technical contributions, the method shows promise in real-world remote sensing contexts. It enables cost-effective extraction of water body boundaries in remote plateau areas. For instance, in ecological monitoring, it can be used to track seasonal and long-term variations in water areas to inform environmental protection policies. In disaster risk management, it aids in detecting dynamic changes in glacial lake shapes, contributing to early warning systems. For water resource evaluation, it facilitates quantitative analysis of regional water volumes and distributions, proving especially valuable in resource-scarce yet high-demand remote regions. These aspects underscore the strategy’s adaptability, particularly for plateau-specific challenges like high sediment loads and intricate background interferences.

Although the proposed method improves performance, limitations persist. The water IoU of 64.84% for Model A2, while a significant improvement, suggests room for enhancement, particularly in highly interfering backgrounds. This is partly attributable to the small size of dataset B, despite data augmentation. Relative to benchmarks in similar studies (e.g., 70% IoU on the LoveDA dataset (Wang et al., 2021)), the results are reasonable for a challenging small-sample plateau setting, but additional data or more advanced augmentation could be beneficial. This study focuses on the pre-train-fine-tune paradigm; future work could incorporate advanced domain adaptation methods (Ganin and Lempitsky, 2015; Tzeng et al., 2017; Long et al., 2015; Ghifary et al., 2016; Saito et al., 2018; Hoffman et al., 2018; Pei et al., 2018), such as adversarial or self-supervised approaches, to further reduce the domain gap with minimal labeling. Extending the framework to other remote sensing tasks, such as building or vegetation extraction, is also a promising direction.

## 5 Conclusion

This study develops a two-stage transfer learning strategy based on the SegFormer model to mitigate domain shift and small-sample challenges in remote sensing image water body segmentation. Validated through the challenging Zhada Tulin case, the proposed strategy elevates the water IoU from 25.50% in direct transfer to 64.84%, substantially surpassing scratch-trained baselines, including SegFormer (37.47%) and the simpler U-Net (48.82%). These findings highlight the effectiveness of pre-training on a diverse source domain followed by targeted fine-tuning. This approach successfully

transfers general water features while adapting to unique local spectral and geomorphological distributions, thereby achieving reliable segmentation under limited-data conditions. In conclusion, this work demonstrates the practical benefits of knowledge reconstruction for remote sensing and offers a robust, cost-effective, and replicable framework highly valuable for thematic information extraction in similar data-scarce environments.

## Declarations

**Author Contributions.** All authors contributed to the study conception and design. Haonan Chen was responsible for the initial investigation, data acquisition, and preprocessing. Building on this foundational work, the formal analysis, methodology development, software implementation, and validation experiments were carried out by Xin Tong. Both authors contributed to the writing, review, and editing of the manuscript and have approved the final version.

**Funding.** The authors declare that no funds, grants, or other support were received during the preparation of this manuscript.

**Data Availability.** The datasets generated and/or analysed during the current study are available from the first author (H.C.) on reasonable request.

**Code Availability.** The source code developed for this study is available from the corresponding author (X.T.) on reasonable request.

**Conflict of Interest.** The authors declare that they have no competing interests.

**Ethics Approval.** Not applicable.

## References

- Badrinarayanan V, Kendall A, Cipolla R (2017) Segnet: A deep convolutional encoder-decoder architecture for image segmentation. *IEEE transactions on pattern analysis and machine intelligence* 39(12):2481–2495
- Chen K, Zou Z, Shi Z (2021) Building extraction from remote sensing images with sparse token transformers. *Remote Sensing* 13(21):4441
- Chen LC, Papandreou G, Kokkinos I, et al (2017) Deeplab: Semantic image segmentation with deep convolutional nets, atrous convolution, and fully connected crfs. *IEEE transactions on pattern analysis and machine intelligence* 40(4):834–848
- Chen LC, Zhu Y, Papandreou G, et al (2018) Encoder-decoder with atrous separable convolution for semantic image segmentation. In: *Proceedings of the European conference on computer vision (ECCV)*, pp 801–818
- Cui Y, Jiang C, Wang L, et al (2022) Mixformer: End-to-end tracking with iterative mixed attention. In: *Proceedings of the IEEE/CVF conference on computer vision and pattern recognition*, pp 13608–13618
- Dosovitskiy A, Beyer L, Kolesnikov A, et al (2020) An image is worth 16x16 words: Transformers for image recognition at scale. *arXiv preprint arXiv:2010.11929*

- Feyisa GL, Meilby H, Fensholt R, et al (2014) Automated water extraction index: A new technique for surface water mapping using landsat imagery. *Remote sensing of environment* 140:23–35
- Ganin Y, Lempitsky V (2015) Unsupervised domain adaptation by backpropagation. In: *International conference on machine learning*, PMLR, pp 1180–1189
- Ghifary M, Kleijn WB, Zhang M, et al (2016) Deep reconstruction-classification networks for unsupervised domain adaptation. In: *Computer Vision–ECCV 2016: 14th European Conference, Amsterdam, The Netherlands, October 11–14, 2016, Proceedings, Part IV* 14, Springer, pp 597–613
- Goodfellow I, Bengio Y, Courville A (2016) *Deep Learning*. MIT Press, Cambridge, MA
- He K, Zhang X, Ren S, et al (2016) Deep residual learning for image recognition. In: *Proceedings of the IEEE conference on computer vision and pattern recognition*, pp 770–778
- Hoffman J, Tzeng E, Park T, et al (2018) Cycada: Cycle-consistent adversarial domain adaptation. In: *International conference on machine learning*, Pmlr, pp 1989–1998
- Huete AR (1988) A soil-adjusted vegetation index (savi). *Remote sensing of environment* 25(3):295–309
- Kass M, Witkin A, Terzopoulos D (1988) Snakes: Active contour models. *International journal of computer vision* 1(4):321–331
- Krizhevsky A, Sutskever I, Hinton GE (2017) Imagenet classification with deep convolutional neural networks. *Communications of the ACM* 60(6):84–90
- LeCun Y, Bottou L, Bengio Y, et al (2002) Gradient-based learning applied to document recognition. *Proceedings of the IEEE* 86(11):2278–2324
- Li R, Zheng S, Zhang C, et al (2021) Multiattention network for semantic segmentation of fine-resolution remote sensing images. *IEEE Transactions on Geoscience and Remote Sensing* 60:1–13
- Liu Z, Lin Y, Cao Y, et al (2021) Swin transformer: Hierarchical vision transformer using shifted windows. In: *Proceedings of the IEEE/CVF international conference on computer vision*, pp 10012–10022
- Long M, Cao Y, Wang J, et al (2015) Learning transferable features with deep adaptation networks. In: *International conference on machine learning*, PMLR, pp 97–105
- Loshchilov I, Hutter F (2017) Decoupled weight decay regularization. *arXiv preprint arXiv:171105101*
- Ma L, Liu Y, Zhang X, et al (2019) Deep learning in remote sensing applications: A meta-analysis and review. *ISPRS journal of photogrammetry and remote sensing* 152:166–177
- McFeeters SK (1996) The use of the normalized difference water index (ndwi) in the delineation of open water features. *International journal of remote sensing* 17(7):1425–1432
- Milletari F, Navab N, Ahmadi SA (2016) V-net: Fully convolutional neural networks for volumetric medical image segmentation. In: *2016 fourth international conference on 3D vision (3DV)*, Ieee, pp 565–571



- Otsu N, et al (1975) A threshold selection method from gray-level histograms. *Automatica* 11(285-296):23–27
- Pan S (2010) Q.: A survey on transfer learning. *IEEE Transactions on Knowledge and Data Engineering* 22(10):1345–1359
- Paszke A (2019) Pytorch: An imperative style, high-performance deep learning library. arXiv preprint arXiv:1912.01703
- Pei Z, Cao Z, Long M, et al (2018) Multi-adversarial domain adaptation. In: *Proceedings of the AAAI conference on artificial intelligence*
- Ronneberger O, Fischer P, Brox T (2015) U-net: Convolutional networks for biomedical image segmentation. In: *Medical image computing and computer-assisted intervention—MICCAI 2015: 18th international conference, Munich, Germany, October 5–9, 2015, proceedings, part III* 18, Springer, pp 234–241
- Rouse Jr J, Haas R, Schell J, et al (1973) Paper a 20. In: *Third earth resources technology satellite-1 symposium: The proceedings of a symposium held by Goddard space flight center at Washington, DC on*, p 309
- Saito K, Watanabe K, Ushiku Y, et al (2018) Maximum classifier discrepancy for unsupervised domain adaptation. In: *Proceedings of the IEEE conference on computer vision and pattern recognition*, pp 3723–3732
- Thapa A, Horanont T, Neupane B, et al (2023) Deep learning for remote sensing image scene classification: A review and meta-analysis. *Remote Sensing* 15(19):4804
- Tuia D, Persello C, Bruzzone L (2016) Domain adaptation for the classification of remote sensing data: An overview of recent advances. *IEEE geoscience and remote sensing magazine* 4(2):41–57
- Tzeng E, Hoffman J, Saenko K, et al (2017) Adversarial discriminative domain adaptation. In: *Proceedings of the IEEE conference on computer vision and pattern recognition*, pp 7167–7176
- Vaswani A, Shazeer N, Parmar N, et al (2017) Attention is all you need. *Advances in neural information processing systems* 30
- Wang J, Zheng Z, Ma A, et al (2021) Loveda: A remote sensing land-cover dataset for domain adaptive semantic segmentation. arXiv preprint arXiv:2110.08733
- Wang L, Li R, Zhang C, et al (2022) Unetformer: A unet-like transformer for efficient semantic segmentation of remote sensing urban scene imagery. *ISPRS Journal of Photogrammetry and Remote Sensing* 190:196–214
- Wang X, Girshick R, Gupta A, et al (2018) Non-local neural networks. In: *Proceedings of the IEEE conference on computer vision and pattern recognition*, pp 7794–7803
- Xie E, Wang W, Yu Z, et al (2021) Segformer: Simple and efficient design for semantic segmentation with transformers. *Advances in neural information processing systems* 34:12077–12090
- Xu H (2006) Modification of normalised difference water index (ndwi) to enhance open water features in remotely sensed imagery. *International journal of remote sensing* 27(14):3025–3033
- Yosinski J, Clune J, Bengio Y, et al (2014) How transferable are features in deep neural networks? *Advances in neural information processing systems* 27
- Yu F, Koltun V (2015) Multi-scale context aggregation by dilated convolutions. arXiv preprint arXiv:1511.07122

- Zhang C, Jiang W, Zhang Y, et al (2022) Transformer and cnn hybrid deep neural network for semantic segmentation of very-high-resolution remote sensing imagery. IEEE Transactions on Geoscience and Remote Sensing 60:1–20
- Zhang L, Zhang L, Du B (2016) Deep learning for remote sensing data: A technical tutorial on the state of the art. IEEE Geoscience and remote sensing magazine 4(2):22–40
- Zhang X, Shang S, Tang X, et al (2021) Spectral partitioning residual network with spatial attention mechanism for hyperspectral image classification. IEEE transactions on geoscience and remote sensing 60:1–14
- Zhang Z, Sabuncu M (2018) Generalized cross entropy loss for training deep neural networks with noisy labels. Advances in neural information processing systems 31
- Zhu XX, Tuia D, Mou L, et al (2017) Deep learning in remote sensing: A comprehensive review and list of resources. IEEE geoscience and remote sensing magazine 5(4):8–36